Original Article

Three-dimensional printing of a patient-specific engineered nasal cartilage for augmentative rhinoplasty

Journal of Tissue Engineering
Volume 10: 1–14

DOI: 10.1177/2041731418824797
journals.sagepub.com/home/tej
SAGE

Hee-Gyeong Yi[1], Yeong-Jin Choi[2], Jin Woo Jung[1], Jinah Jang[3,4], Tae-Ha Song[5], Suhun Chae[1], Minjun Ahn[1], Tae Hyun Choi[6], Jong-Won Rhie[7] and Dong-Woo Cho[1]

Abstract

Autologous cartilages or synthetic nasal implants have been utilized in augmentative rhinoplasty to reconstruct the nasal shape for therapeutic and cosmetic purposes. Autologous cartilage is considered to be an ideal graft, but has drawbacks, such as limited cartilage source, requirements of additional surgery for obtaining autologous cartilage, and donor site morbidity. In contrast, synthetic nasal implants are abundantly available but have low biocompatibility than the autologous cartilages. Moreover, the currently used nasal cartilage grafts involve additional reshaping processes, by meticulous manual carving during surgery to fit the diverse nose shape of each patient. The final shapes of the manually tailored implants are highly dependent on the surgeons' proficiency and often result in patient dissatisfaction and even undesired separation of the implant. This study describes a new process of rhinoplasty, which integrates three-dimensional printing and tissue engineering approaches. We established a serial procedure based on computer-aided design to generate a three-dimensional model of customized nasal implant, and the model was fabricated through three-dimensional printing. An engineered nasal cartilage implant was generated by injecting cartilage-derived hydrogel containing human adipose-derived stem cells into the implant containing the octahedral interior architecture. We observed remarkable expression levels of chondrogenic markers from the human adipose-derived stem cells grown in the engineered nasal cartilage with the cartilage-derived hydrogel. In addition, the engineered nasal cartilage, which was implanted into mouse subcutaneous region, exhibited maintenance of the exquisite shape and structure, and striking formation of the cartilaginous tissues for 12 weeks. We expect that the developed process, which combines computer-aided design, three-dimensional printing, and tissue-derived hydrogel, would be beneficial in generating implants of other types of tissue.

Keywords

Three-dimensional bioprinting, rhinoplasty, tissue engineering, decellularization, computer aided design and manufacturing

Date received: 27 July 2018; accepted: 23 December 2018

[1]Department of Mechanical Engineering, Pohang University of Science and Technology (POSTECH), Pohang, Korea
[2]Division of Integrative Biosciences and Biotechnology, Pohang University of Science and Technology (POSTECH), Pohang, Korea
[3]Department of Creative IT Engineering, Pohang University of Science and Technology (POSTECH), Pohang, Korea
[4]School of Interdisciplinary Bioscience and Bioengineering, Pohang University of Science and Technology (POSTECH), Pohang, Korea
[5]Medical Device Development Center, Daegu-Gyeongbuk Medical Innovation Foundation (DGMIF), Daegu, Korea
[6]Department of Plastic and Reconstructive Surgery and Institute of Human Environment Interface Biology, Seoul National University Children's Hospital, Seoul National University College of Medicine, Seoul, Korea
[7]Department of Plastic Surgery, College of Medicine, The Catholic University of Korea, Seoul, Korea

Corresponding author:
Dong-Woo Cho, Department of Mechanical Engineering and Center for Rapid Prototyping-based 3D Tissue/Organ Printing, Pohang University of Science and Technology (POSTECH), 77 Cheongam-ro, Nam-gu, Pohang, Kyungbuk 37673, Korea.
Email: dwcho@postech.ac.kr

Introduction

Rhinoplasty, which corrects and reconstructs the form and function of the nose for therapeutic and cosmetic purposes, is one of the most popular plastic surgeries.[1] In the common procedure of dorsal augmentative rhinoplasty, a nasal implant is inserted into a pocket generated in a subperiosteal region.[1] There are two major types of nasal implants used for this surgery: the autologous cartilage graft and the synthetic nasal implant.[2] Autologous cartilage grafts harvested from rib and ear cartilages are ideal materials.[2] However, the autologous transplantation has drawbacks of limited tissue source, long surgery time, and donor site morbidity.[2] Nasal implants made of synthetic material (e.g., silicone or polytetrafluoroethylene) are abundantly available, provided as ready-made products, and do not require additional surgery to obtain autologous tissue.[2,3] Surgeons and patients have widely chosen the synthetic nasal implants for permanent nasal augmentation, in spite of the risks of inflammatory responses caused by foreign material.[2] However, the prefabricated form of the synthetic nasal implants still requires manual carving with a sharp knife in the operating room, to fit the implant to the contour of the host nasal cartilage.[1] The manual carving procedure involves a surgeon's skills and experience and cannot guarantee construction of the desired shape of the nose. [4–7] The manual procedure often results in an inappropriate implant shape that causes an unsatisfactory nose shape and an unstable assembly of host tissue implant with a high risk of extrusion of the implant through the skin.[8]

Three-dimensional (3D) printing is an emerging technology in the field of tissue engineering and regenerative medicine due to its benefits of constructing an implant with a patient-specific design based on computer-aided design and manufacturing (CAD/CAM) processes.[9] In a preoperative consultation for a patient undergoing rhinoplasty, virtual surgery simulation software is widely used to determine a reconstructed nasal shape for the patient.[10] Based on the desired reconstructed nasal shape, the geometrical differences in shape and size can be digitally calculated, and the customized nasal implant can be produced by 3D printing technology, including CAD/CAM. Since the virtual simulation software provides a postoperative facial model based on computer graphics, it is possible to predict the augmented nose shape and the overall facial balance. Therefore, a 3D-printed nasal graft would achieve the shape of nose with minimized error from the virtual nasal model in simulation, due to the coincidence of shape and size between the printed and designed objects.

In addition, the 3D printing technique allows various materials to be constructed by freeform fabrication, which involves a selection of biomaterials effective for the regeneration of specific tissue. The traditional synthetic nasal implants are permanently present in the patient's body and can cause a variety of complications, including infection and immune reactions.[8] A 3D-printed nasal implant can be regarded as a suitable graft for augmentative rhinoplasty, as it can be designed to meet the patient's specific shape and is made of selected biodegradable materials to reduce complications.

Hydrogels—including silk fibroin,[11] alginate,[12] fibrin,[13] and decellularized extracellular matrix (dECM)-derived hydrogel[14]—have been used as 3D scaffolding materials for cells, owing to their extracellular matrix (ECM)-like environment that promotes cell growth and maturation. Among these hydrogels, dECM-derived hydrogels that retain tissue-specific biochemical cues have been shown to have excellent regenerative capability.[15] Despite this capacity, dECM-derived hydrogels usually have poor self-supporting ability due to low viscosity and mechanical properties, which inevitably hinders their ability to be made into large and complex 3D structures.[16]

Here, a nasal cartilage implant with a customized design was engineered by serial processes, including 3D printing of a nasal implant and an injection of cell-laden hydrogel for augmentative rhinoplasty application. An algorithm was applied to analyze the shapes of preoperative and virtual postoperative noses and to generate the 3D exterior shape of the customized nasal implant. Using CAD software, octahedral interior architecture was included in the model of the nasal implant. A cartilage-derived hydrogel was applied to formulate a mixture of human adipose-derived stem cells (hASCs) and the hydrogel, and an injection technique was established to fill the interior architecture of the nasal implants with the cell-laden hydrogel. Differentiation of the hASCs into a chondrogenic lineage in the cartilage-derived hydrogel and formation of the cartilaginous matrix in the engineered nasal cartilage implant *in vitro* were assessed. In addition, the engineered nasal cartilage implanted in mouse subcutaneous region showed striking cartilage tissue formation and native tissue–like biological characteristics in the 3D-printed customized structure. The engineered nasal cartilage implant exhibited valuable benefits in cartilage regeneration, by achieving the merits of both an autologous nasal graft and a synthetic nasal implant. Therefore, we expect that the developed process combining CAD, 3D printing, and the use of cartilage-derived hydrogel will also be favorable for generating implants of other types of tissue.

Materials and methods

Generation of 3D custom-design of nasal implants

FaceGen software (Singular Inversions Inc, ON, Canada) was used to convert two-dimensional (2D) facial pictures (front and side views) into a 3D facial model and to reconstruct the face, including the nose. Figure 1(a) shows the

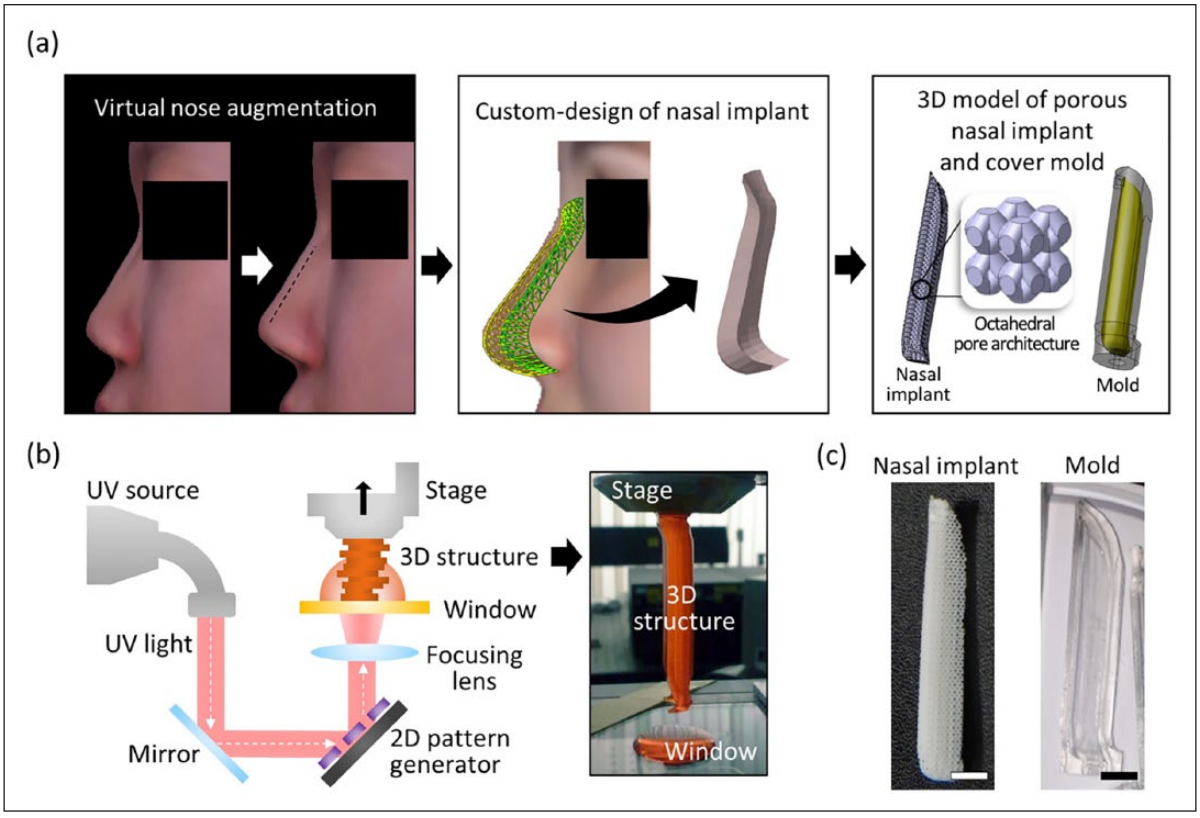

Figure 1. Computer-aided design and 3D printing of a patient-customized nasal implant. (a) The process of generating the custom design of the nasal implant model. The difference between the preoperative and postoperative nose geometrical shapes was calculated. A 3D solid model was then generated according to the geometric difference. Finally, an octahedral pattern architecture was designed in the nasal implant model, and a cover mold model was designed based on the nasal implant model. (b) Schematic elucidating the principle of fabricating a 3D construct by the pMSTL system. (c) Photographs of the fabricated PCL nasal implant and OrmoComp cover mold with the patient-specific design (scale bars = 5 mm).

3D facial model that was obtained, with an augmented nose. An algorithm developed for this study generated the nasal graft model using the two nasal surface data extracted from the original and modified nasal model. The facial models (with original and augmented noses) were transformed into mesh surface models. In each surface model, arbitrary regions were set around the nose, and matrices were generated for the x, y, and z coordinate values of each node in the corresponding regions. The external shape of the nasal implant was generated by calculating the difference between the two matrices (Supplementary Figure 1). Minor factors (e.g., thinned skin or compressed implant) that can cause volumetric change of the postoperative nose were ignored. The generated model surface data were exported to a stereolithography (STL) file format consisting triangular meshes. InStep software (Solveering™ LLC, Albuquerque, NM, USA) was used to convert the surface data of the STL file format to a solid model of STEP file format. The interior architecture (octahedral shape, unit size: 2 mm × 2 mm × 2 mm, strut width: 300 μm) was designed in a previous study[6] and was combined with the nasal graft model to generate the octahedral interior architecture of the nasal implants.

3D printing process of the custom-designed framework and cover molds

Figure 2(b) shows the process of fabricating the nasal implant and its cover mold. The projection-based microstereolithography (pMSTL) prints a 3D object through an additive manufacturing process, by vertically stacking ultraviolet (UV)-cured 2D image patterns. The sacrificial mold model was designed by the previous process.[6] The mold model was exported to STL file format and later converted to bitmap images cross-sectioned at intervals of 50 μm by the previously developed algorithm.[17] An alkali-soluble photopolymer[18] was used to make the sacrificial mold, then the uncured resin was washed in an isopropyl alcohol (IPA)-stirred environment for half a day. A polycaprolactone (PCL)/chloroform solution (150:100 w/w) was injected into the pores of the mold, and the sacrificial mold was immersed in a stirred IPA solution for 12 h, to

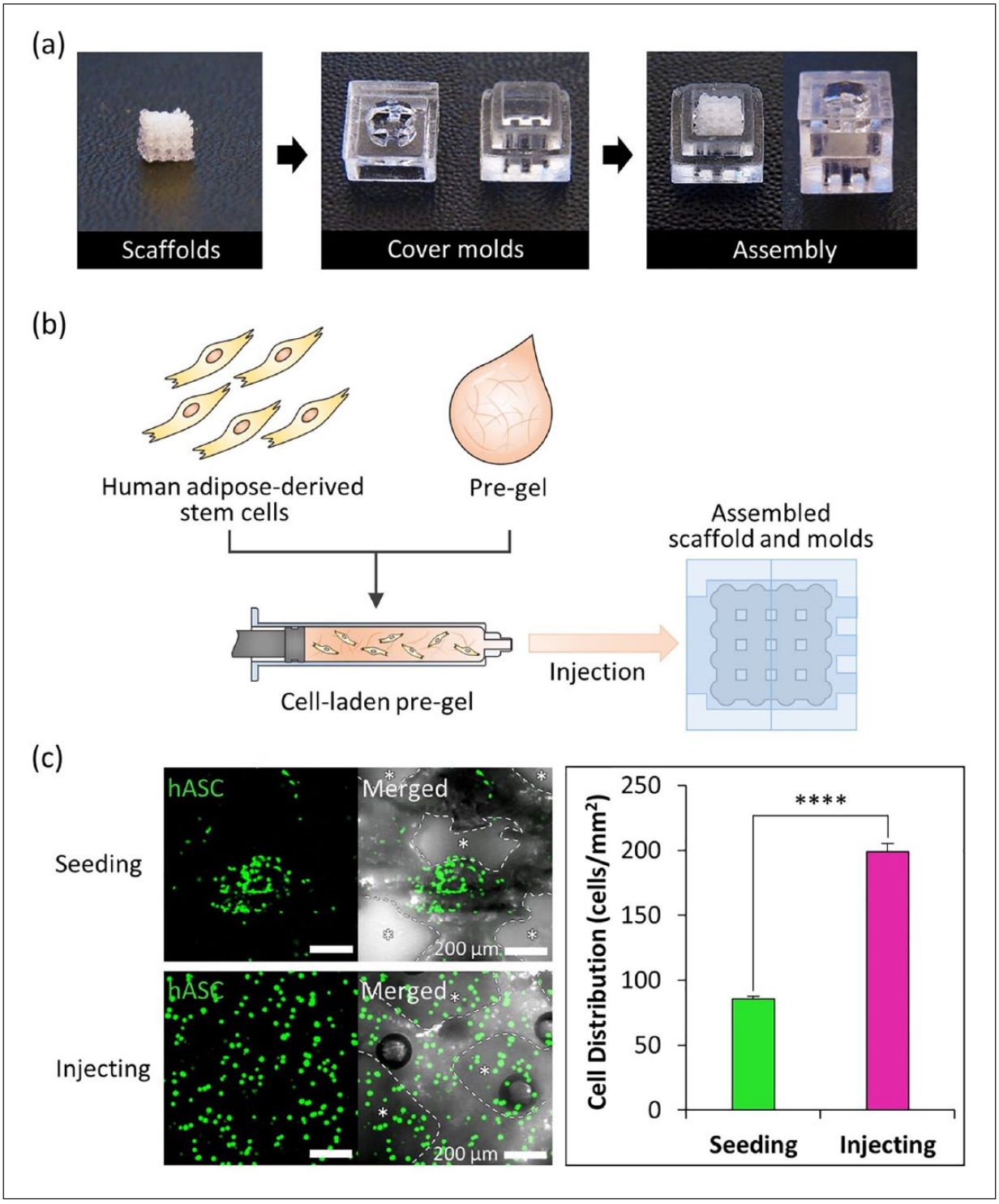

Figure 2. Process of cell-laden hydrogel injection technique and cell distribution in the scaffold. (a) Assembling cover molds and scaffolds for cell-laden hydrogel injection. (b) A schematic of the cell-laden hydrogel pre-gel injection procedure. (c) Calcein AM staining of each scaffold after cell seeding and injecting (scale bar = 200 μm, left). Quantification of cell distribution in each scaffold (n = 3 per experimental group, $^{****}p < 0.0001$, right).

remove the chloroform solution and harden the PCL. The PCL nasal implant was obtained by dissolving the sacrificial mold in 0.5 N NaOH for 12 h.

The cover molds were printed with a biocompatible UV-curable resin[19] (Ormocomp, Micro Resist Technology GmbH, Berlin, Germany), in pMSTL system. The uncured

resin was washed in a stirred IPA solution for a day and post-cured in a UV chamber for 12 h.

Cell isolation and culture

The hASCs were isolated from a single donor after obtaining informed consent. The experiment using hASCs was conducted in accordance with the Institutional Review Board of Seoul St. Mary's Hospital, The Catholic University of Korea (KC11TNMS0095). The adipose tissue from the patient was digested with 0.05% type I collagenase at 37°C for 30 min. After centrifugation of the digested tissue at 1000 r/min for 5 min, the cell pellet was collected and filtered through a 100 μm nylon mesh to remove debris. The isolated cells were then plated on a 100-mm culture dish and cultured in growth medium containing low glucose Dulbecco's modified eagle's medium (DMEM; Hyclone, Logan, UT, USA), 10% fetal bovine serum (FBS, Hyclone, Logan, UT, USA), 100 U/mL penicillin, and 100 μg/mL streptomycin (Hyclone, Logan, UT, USA), and incubated at 37°C in a humidified atmosphere of 5% CO_2. The growth medium was refreshed every 2–3 days. All experiments were conducted with the hASCs prior to passage 5.

Preparation of cartilage-derived hydrogel

Hyaline cartilages were collected from porcine knee parts obtained from a local butcher and chopped into tiny pieces (less than 3 mm^2 in size). The cartilages were decellularized, and cartilage-decellularized ECM pregel was prepared, following the protocol that was previously described.[15] Briefly, the tissue pieces were placed in a hypotonic buffer solution (10 Mm Tris-HCL, pH 8.0), subjected to six freeze-thaw cycles (frozen at −80°C, and thawed at 37°C), treated with 0.25% trypsin at 37°C for 24 h, washed with a hypertonic buffer solution (1.5 M NaCl in 50 mM Tris-HCL, pH 7.6), treated with a nuclease solution (50 U/mL DNase and 1 U/mL RNase in 10 mM Tris-HCL, pH 7.5) at 37°C for 4 h, treated with 1% Triton X-100 solution for 24 h, then washed with phosphate-buffered saline (PBS) >72 h to remove all the enzymes and detergents. A viscous pregel solution was obtained following the procedures; the decellularized tissues were lyophilized by grinding with the help of liquid nitrogen. The ground tissues were solubilized in 0.5 M acetic acid solution containing pepsin (1 mg pepsin per 10 mg tissue) for 48 h, and neutralized with 10 M NaOH.

Injection of cell-laden hydrogels into the framework

The hASCs were harvested by treating with 0.25% trypsin/0.01% ethylenediaminetetraacetic acid (EDTA) solution (Gibco-BRL, Grand Island, NY, USA), and cell-suspended growth medium was prepared. The cell-suspended medium was mixed with a medium-viscosity alginate and a cartilage pre-gel solution containing 500 U /mL tyrosinase on ice to complete the concentration of 1×10^7 cells/mL of the cells, 2% (w/v) of the alginate, and 3% (w/v) of the cartilage-derived hydrogel. After cover molds and a PCL-framework were assembled, the cell-alginate-cartilage-derived hydrogel mixture was injected into the inlet of the cover molds, using a 1-ml syringe. To cross-link the alginate, the assembled construct was first immersed in a 100 mM $CaCl_2$ bath for 20 min. Then the cell-injected framework was disassembled from the cover molds, washed twice with PBS, and incubated at 37°C for 1 h to cross-link the tyrosinase-included cartilage-derived hydrogel. The cell-injected framework was cultured in chondrogenic differentiation medium containing high glucose DMEM (Hyclone, Logan, UT, USA), 10% FBS, 100 U/mL penicillin, 100 μg/mL streptomycin (Hyclone, Logan, UT, USA), 10 nM dexamethasone (Sigma Aldrich, St. Louis, MO, USA), 50 μg/mL ascorbate-2-phosphate (Sigma Aldrich, St. Louis, MO, USA), 6.25 μg/mL insulin-transferrin-selenium (Gibco, Grand Island, NY, USA), and 10 ng/mL transforming growth factor β1 (BD Bioscience, San Diego, CA, USA). The medium was refreshed every 2–3 days.

Real-time polymerase chain reactions

To compare changes in the chondrogenic potential of the hACSs encapsulated in each hydrogel, the fold-increase in the mRNA expression of the representative chondrogenic markers, including sex determining region Y-box 9 (*SOX9*), aggrecan (*ACAN*), and type II collagen (*COL2A1*), was determined relative to the mRNA expression of the housekeeping gene glyceraldehyde 3-phosphate dehydrogenase (*GAPDH*). From each construct (n = 4 per experimental group), mRNA was isolated using an RNeasy Plant Mini Kit (QIAGEN, Venlo, Netherlands), following the manufacturer's instructions. Complementary DNAs (cDNAs) were synthesized using the mRNA templates and a Maxima First Strand cDNA Synthesis Kit for quantitative reverse transcription polymerase chain reaction (RT-qPCR; Thermo Fisher Scientific, Waltham, MA, USA). After preparing the mixtures of the cDNAs, the primers of the target genes and an SYBR Green PCR Master Mix assay (Applied Biosystems, Waltham, MA, USA), RT-qPCR was performed using an ABI StepOnePlus system (Applied Biosystems, Waltham, MA, USA). The reaction plates were heated to 95°C for 10 min and underwent 40 cycles of denaturation at 95°C for 15 s and annealing at 60°C for 1 min. The primer sequences were designed as previously reported,[20] and the details are described in Supplementary Table 1. The fold-increases of target genes were estimated using the $2^{-(\Delta\Delta c(t))}$ method.

Quantification of glycosaminoglycan and DNA

The production of glycosaminoglycan (GAG) was measured, normalized with the amount of DNA at the initial day and days (1, 7, 14, and 21). The digest from each construct (n = 3 per experimental group) was obtained after reaction with 125 μg/mL papain (Sigma Aldrich, St. Louis, MO, USA) in 0.1 M sodium phosphate, 10 mM disodium EDTA (Na_2-EDTA), and 10 mM L-cysteine hydrochloride (pH 6.5) at 60°C for 16 h. After centrifugation of the digests, the supernatant per construct was collected. The total DNA content per construct was estimated from the fluorescence intensity at an excitation wavelength of 360 nm and an excitation wavelength of 465 nm using the bisbenzimidazole dye-bound aliquot (Hoechst 33258; Sigma Aldrich, St. Louis, MO, USA) and a microplate reader (SpectraMax, Molecular Devices, CA, USA). The amount of GAG was quantified by reading the absorbance at a wavelength of 490 nm, using the 1,9-dimethyl methylene blue-bound aliquot and spectrophotometry (Wallac 1420, PerkinElmer, Waltham, MA, USA).

Immunofluorescence staining

The chondrogenic differentiation of the hASC encapsulated in each gel was analyzed through the immunofluorescence staining of aggrecan and type 2 collagen. The samples were fixed with 4% paraformaldehyde for 10 min. The samples were then permeabilized with 0.1% Triton X-100 solution for 5 min, blocked with 1% bovine serum albumin solution for 1 h. The both of anti-aggrecan antibody (Abcam) and anti-type 2 collagen antibody (Abcam) were diluted in PBS at the ratio of 1:100 and treated to the samples at 4°C for overnight. After washing the samples with PBS, the DAPI (1:500) and the secondary antibodies (1:200) diluted in PBS were treated to the samples at 4°C for overnight. The samples were then observed under a confocal microscopy.

In vivo experiments

To evaluate the formation of cartilage in the *in vivo* microenvironment, tissue-engineered nasal cartilages were implanted in the subcutaneous region of the mice after a day of stabilization of the cell-injected frameworks with chondrogenic differentiation medium (one implant per mouse, three mice per experimental group). Constructs were inserted into a pocket made on the back of a 4-week-old female athymic (nu/nu) BALB/C mouse. The pocket was sutured and coated with an antibiotic ointment. All experiments were conducted in a specific pathogen-free room. After euthanasia of the mice by administration of a CO_2 overdose at 6 or 12 weeks, the constructs were retrieved. All of the animal studies were approved by the Institutional Animal Care and Use Committee (IACUC) at POSTECH Biotech Center, Pohang University of Science and Technology (Approval number: 2015-0025).

Histological analysis

Following retrieval from the mice, the implants were harvested, and fixed in 10% formalin, then embedded in paraffin, and sectioned at 4 μm. Sections were stained with hematoxylin and eosin (H&E) and Masson's trichrome for examination of tissue regeneration. Accumulation of collagen type II was assessed by immunohistochemistry to identify the cartilage matrix tissue formation. Sections were blocked with 10% goat serum for 30 min, and incubated overnight at 4°C with a 1:100 dilution of anti-human type II collagen antibody (Merck Millipore, Darmstadt, Germany). The biotinylated secondary antibody was applied for 30 min at room temperature. Sections were rinsed and an avidin and biotinylated horseradish peroxidase complex (VECTASTAIN Elite ABC reagent; Vector Laboratories, Burlingame, CA, USA) was applied for 30 min at room temperature. The 3, 3-diaminobenzidine peroxidase substrate (Vector Laboratories, Burlingame, CA, USA) was treated for color development. All samples were counterstained with hematoxylin to observe the nuclei.

Statistics

The quantified experimental data are presented as the mean ± standard deviation (SD). The statistical significance was calculated using a two-tailed Student's t-test for the comparison of two groups. In addition, we applied a one-way analysis of variance (ANOVA) for the comparison of more than three groups. The differences were regarded as significant at $p < 0.05$.

Results

Fabrication of the nasal implant framework and cover mold

Augmentative rhinoplasty aims to increase the overall volume of the nose, with the pronasale as the center. Here, the algorithm generated the exterior shape of the nasal implant model by calculating the difference between the virtual augmented postoperative nose and the original nose. The CAD created the interior octahedral architecture in the final 3D nasal implant model. Based on the 3D nasal implant model, the nasal implant was fabricated by a 3D printing technique. The slope and dimension of the 3D-printed nasal implant will vary according to the individual's nasal shape. Here, we printed the nasal implant based on a specific patient's facial geometry data. The resulting nasal implant was 38.2 mm × 7.3 mm × 6.1 mm (L × W × H) in size. To support the injected cell-laden hydrogel, an octahedral pore (2 mm × 2 mm × 2 mm unit size) was incorporated into the

nasal implant. Since the porosity, the fraction of the volume of the octahedral space over the total volume, affects the flexibility of the nasal implant, we compared 50% and 70% porosities through a three-point bending test. The 70% porosity showed more elastic characteristics in the load–displacement curve than did the 50% porosity (Supplementary Figure 2). Therefore, we selected 70% porosity to achieve excellent stability of the implant to endure external stimuli (e.g., skin tension) at an implanted site. The cover molds of the nasal implant were composed of two parts for assembly. The assembled mold had a volume of 44.5 mm × 10.4 mm × 10.1 mm (L × W × H). The mold cavity had a 0.2 mm offset volume expanded over the implant model. The mold was placed on one part of the cover mold, and the other part was press-fitted.

Evaluation of the cell-laden hydrogel injection technique

To test the cell-laden hydrogel injection technique, the cubic shape scaffolds and the cover molds were printed with the same process as that used for the nasal implant (Figure 2(a)). The scaffolds had a volume of 6 mm × 6 mm × 6 mm, and the cover molds had a 2 mm × 2 mm × 2 mm unit size. The mold parts and scaffolds were assembled, and no leakage was observed during the injection of hASCs-laden hydrogel using a 1.0-mm syringe (Figure 2(b)). Qualitative analysis of the cell distribution from the injection technique showed a 2.3-fold higher seeding efficiency and more uniform cell distribution than those with the common cell seeding (Figure 2(c)).

Preparation of an engineered nasal cartilage

The cover molds and the nasal implants were successfully assembled and enabled the injection of hASC-laden hydrogel into the nasal implants to generate the engineered nasal cartilage (Figure 3(a)). Since the 3D-printed nasal implant had a large volume (38.2 × 7.3 × 6.1 mm (L × W × H)), the cell viability and hypoxia generation were evaluated through both LIVE/DEAD and pimonidazole staining, respectively. A substantial number of living cells were evenly distributed throughout the interior architecture of the nasal implants. Cells in both the alginate and the cartilage-derived hydrogel maintained high viability in a long-term culture (Figure 3(b)). The cell viability of the alginate hydrogel group was 89.9 ± 2.3%, 87.7 ± 1.8%, and 90.6 ± 2.3% at 4, 10, and 14 days, respectively. The cartilage-derived hydrogel group showed 90.9% ± 1.8%, 88.5% ± 1.6%, and 89.1% ± 2.5% at 4, 10, and 14 days, respectively. Hypoxia was rarely observed in either the innermost or outermost regions of the alginate and the cartilage-derived hydrogels, indicating that sufficient nutrients and oxygen had diffused through the hydrogel-containing cells in the interior architecture of the implants (Figure 3(c)).

Cartilage differentiation in the engineered nasal cartilage in vitro

After the establishment of the cell-laden hydrogel injection technique, the capability of using the cartilage-derived hydrogel with the alginate hydrogel for inducing chondrogenesis in the nasal implant was evaluated. First, the expression levels of *SOX9, ACAN*, and *COL21A* (the genes related to the early chondrogenic differentiation process) were assessed. The cells injected with the cartilage-derived hydrogel showed significantly higher expression levels of all three genes from day 14, compared to expression levels in the alginate hydrogel (Figure 4(a)). The differences in genetic expression between alginate and cartilage-derived hydrogels at day 21 became greater than the differences at day 14. When normalized to DNA, the measurements showed that the GAG levels were higher in the cartilage-derived hydrogel group than in the alginate hydrogel group at all experimental time points (Figure 4(b)). The values of GAG/DNA in the alginate hydrogel group for the experimental period showed insignificant differences as time progressed. The greatest difference in GAG/DNA between the two groups was observed at day 14. In addition, the cartilage-derived hydrogel group contained more cells producing either aggrecan or type-2 collagen than the cells in the alginate group (Figure 4(c) and (d)). Although there was some inconsistency between the genetic expression analysis and the GAG production measurement along the culture period, it was demonstrated throughout the *in vitro* assays that the cartilage-derived hydrogel had a higher potential for cartilage differentiation than did the alginate hydrogel.

Neo-cartilage formation in the engineered nasal cartilage in vivo

The results confirmed that the engineered nasal cartilage was well retained under *in vivo* conditions that surrounded it with physical stress. A subcutaneous region was chosen for the implantation of the engineered nasal cartilages in mice to simulate the physical stresses occurring at a location beneath a skin layer (Figure 5(a)). The engineered nasal cartilage was subjected to various mechanical stresses, including skin tension and flexure due to the natural bending motion. During the implantation period, the appearance of the implanted site maintained the augmented shape, without noticeable deformation. After 12 weeks, the engineered nasal cartilages were retrieved, and no damage induced by the physical environment surrounded the implants was observed (Figure 5(b)). In addition, the implants were covered with blood vessels and fully filled with neo-tissues (Figure 5(b), enlarged images).

Cartilage tissue formation in the engineered nasal cartilages on 6 and 12 weeks post-implantation was evaluated. Given, the results from *in vitro* analyses, a comparison was

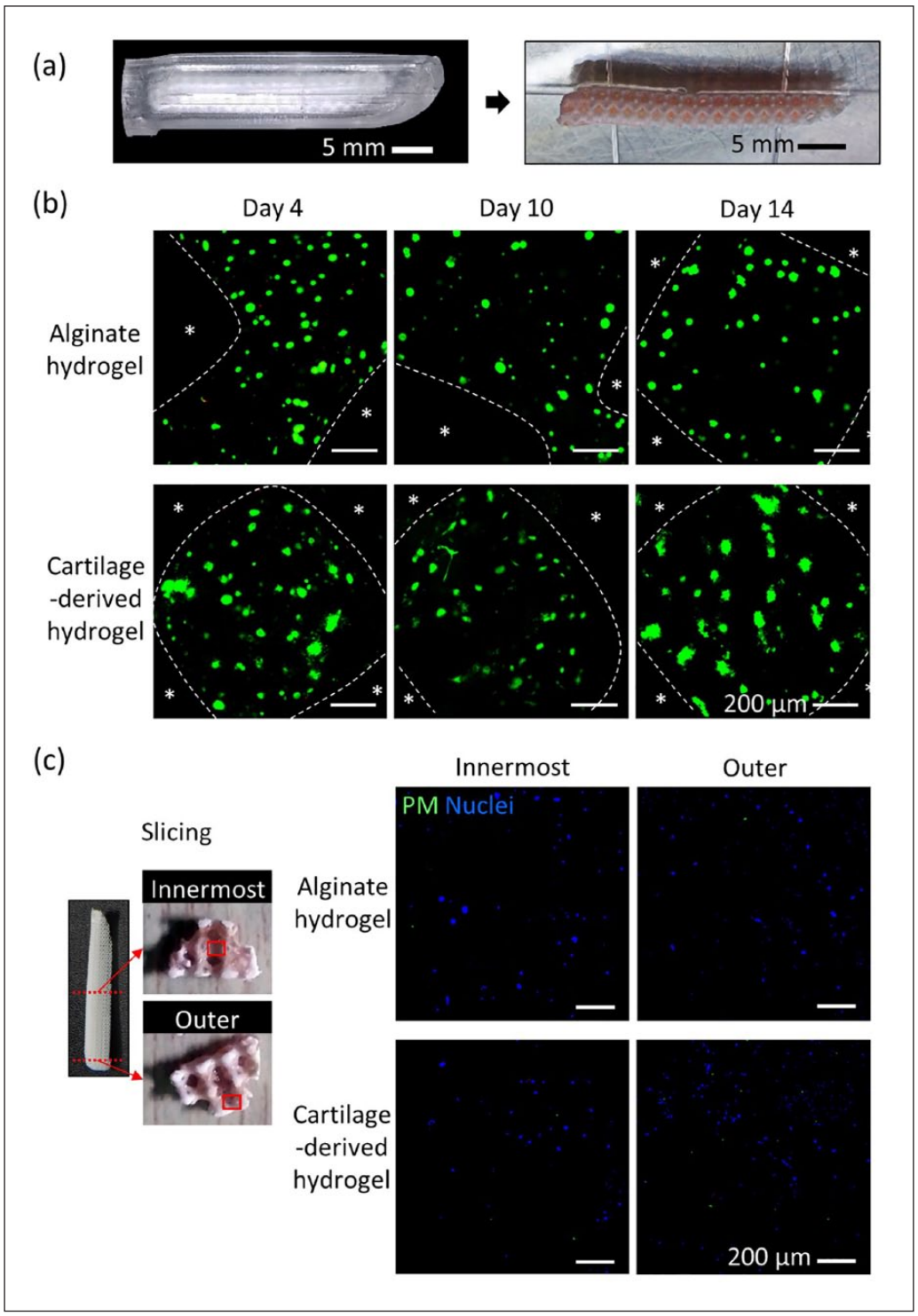

Figure 3. Cell viability and hypoxia in engineered nasal cartilage. (a) Assembled nasal implant and cover mold (left); hydrogel-injected nasal implant (right). (b) LIVE/DEAD staining of engineered nasal cartilage at days 4, 10, and 14. Star symbols indicate PCL region, green indicates live cells, and red indicates dead cells in the hydrogel region (scale bar = 200 μm). (c) Pimonidazole staining of engineered nasal cartilage at day 14: green indicates hypoxia, and blue indicates nucleus (DAPI; scale bar = 200 μm).

made between the cartilage-derived hydrogel-injected group and the alginate hydrogel–injected group. In the first 6 weeks, the cartilage-derived hydrogel-injected group presented faster formation of cartilage tissues compared to the alginate hydrogel group, as detected through the H&E staining and immunohistochemistry of type-2 collagen (Figure 6). The

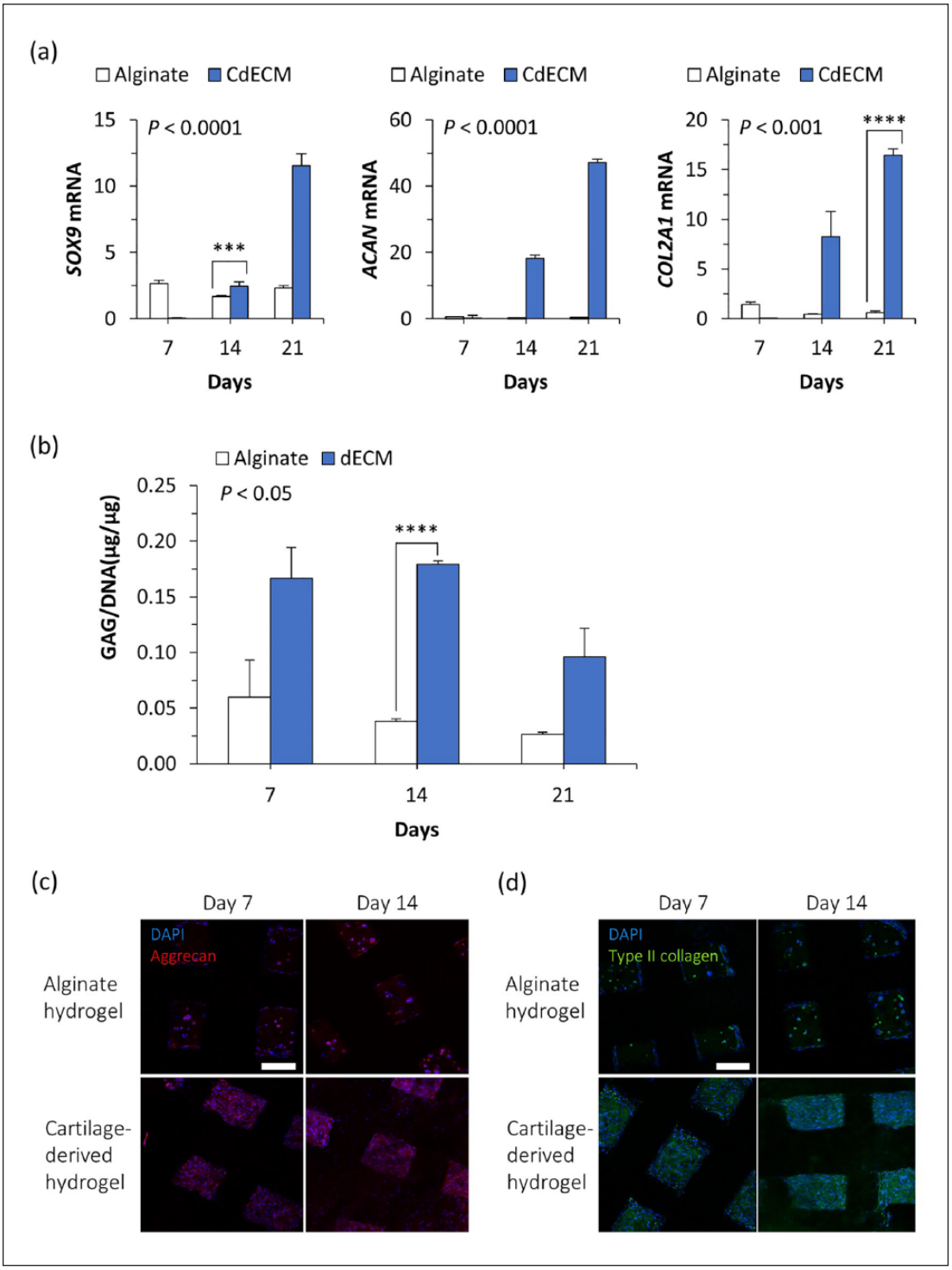

Figure 4. Chondrogenic differentiation in engineered cartilage *in vitro*. (a) Changes in mRNA expression levels and (b) GAG amount normalized to DNA amount, and the production of (c) aggrecan and (d) type-2 collagen in the hASCs injected with alginate hydrogel or cartilage-derived hydrogel (n = 4 per experimental group for real-time qPCR; n = 3 per experimental group for biochemical assay; ***$p < 0.001$; ****$p < 0.0001$; scale bar = 200 μm).

H&E-stained images showed the outstanding formation of lacunae, a representative histological marker of cartilage tissue, in the cartilage-derived hydrogel-injected implants, while fewer of the hASCs injected with alginate gel differentiated into chondrocytes, and thus formed fewer lacunae. Moreover, the cartilage-derived hydrogel group exhibited a

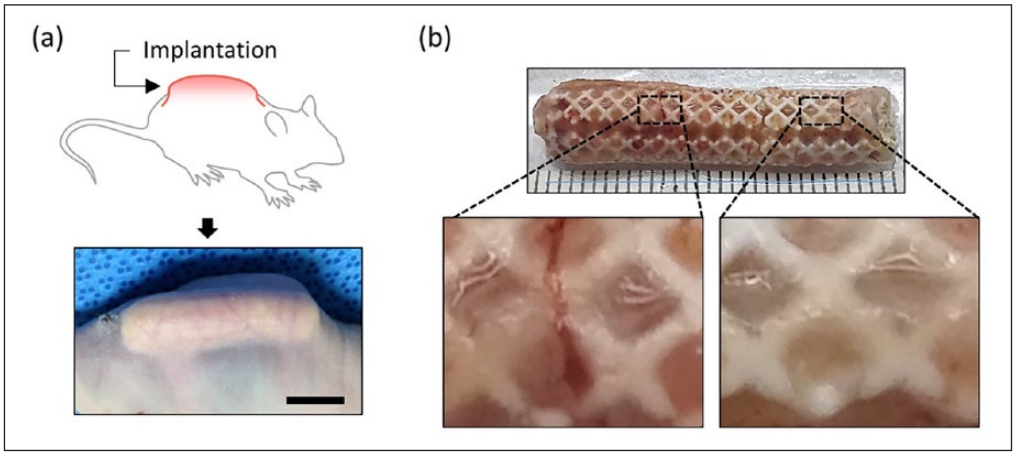

Figure 5. Subcutaneous implantation of the engineered nasal cartilage: (a) schematic and photograph of the construct implanted in a dorsal subcutaneous region (scale bar = 10 mm) and (b) gross image of the retrieved implant after 12 weeks post-implantation. The ruler is graduated in mm.

stronger orange-red deposit than the alginate group in Safranin O staining, indicating the higher proteoglycan and GAG production than that of alginate hydrogel group (Supplementary Figure 3). The samples from the cartilage-derived hydrogel-injected group showed highly concentrated blue color with Masson's Trichrome staining, indicating collagen deposition (Supplementary Figure 4). The samples from the alginate group showed less collagen-positive blue color for all experimental periods. More specifically, compared to the alginate group, the cartilage-derived hydrogel-injected group showed a wider and more intense brown color that indicates the secretion of type II collagen (Figure 6). In addition, blood vessel networks were not observed in the inner region of the implants, except for the surface. Therefore, compared to alginate hydrogel, the cartilage-derived hydrogel was more beneficial for inducing chondrogenic differentiation of the encapsulated hASCs in the subcutaneous environment.

Discussion

Currently, augmentative rhinoplasty is a very popular cosmetic surgery in Asia.[1,3] Most of the nasal implants—including autologous cartilage and synthetic grafts—are modified through manual trimming during augmentative rhinoplasty, to meet the patient's desired shape.[2,3,7] Therefore, the postoperative nasal shape is closely related to the surgeon's subjectivity, experience, and skill. As a result, over 16% of patients are dissatisfied with the results of their surgery, or are hoping for reoperation.[2,21] Moreover, surgical failures associated with undesired nose shape, immune rejection, and infection have become a major social problem.[22,23] Although autologous cartilages have been shown to produce excellent engraftment, they have limitations, such as the need for additional surgery, the poor capacity of self-regeneration, high donor site morbidities, and their limited availability.[2,24]

This study suggests a new paradigm for the process from initial cosmetic consultation to the operation of augmentative rhinoplasty, as follows: (1) in the preoperative consultation, the desired shape of nose would be designed with facial editing software based on the patient's needs; (2) the nasal implant model generation algorithm and CAD create a nasal implant model that can achieve the desired nose shape; (3) after consultation, the 3D-printed nasal implant would be fabricated without concern for the surgeon's proficiency; (4) the surgeons would mix hASCs extracted from lipoaspirate and the hydrogel, and immediately prepare the engineered nasal cartilage, by simply injecting the cell-laden hydrogel into the 3D-printed nasal implant in the operating room; and (5) the engineered nasal cartilage would be implanted into the patient and may eventually be transformed into autologous-like cartilage tissue that maintains its initially determined nose shape. This new process can shorten the additional operation time for implant preparation (harvesting the autologous tissue or carving the synthetic implant), and it will be a comfortable and convenient process for both the patients and the surgeons.

The nasal implant was designed by calculating the volume difference between the preoperative nose and expected postoperative nose through the algorithm developed in this study. However, external pressure generated by the extended skin tissue can affect the final shape of the nose, which can cause patient dissatisfaction. If the implant is considerably harder than the skin tissue, the external pressure may be negligible, but a hard implant can cause additional complications, such as graft extrusion.[3] The improved algorithm presented here can predict and compensate for the shape changes of the nose that may develop. Shape changes can also occur along with the degradation

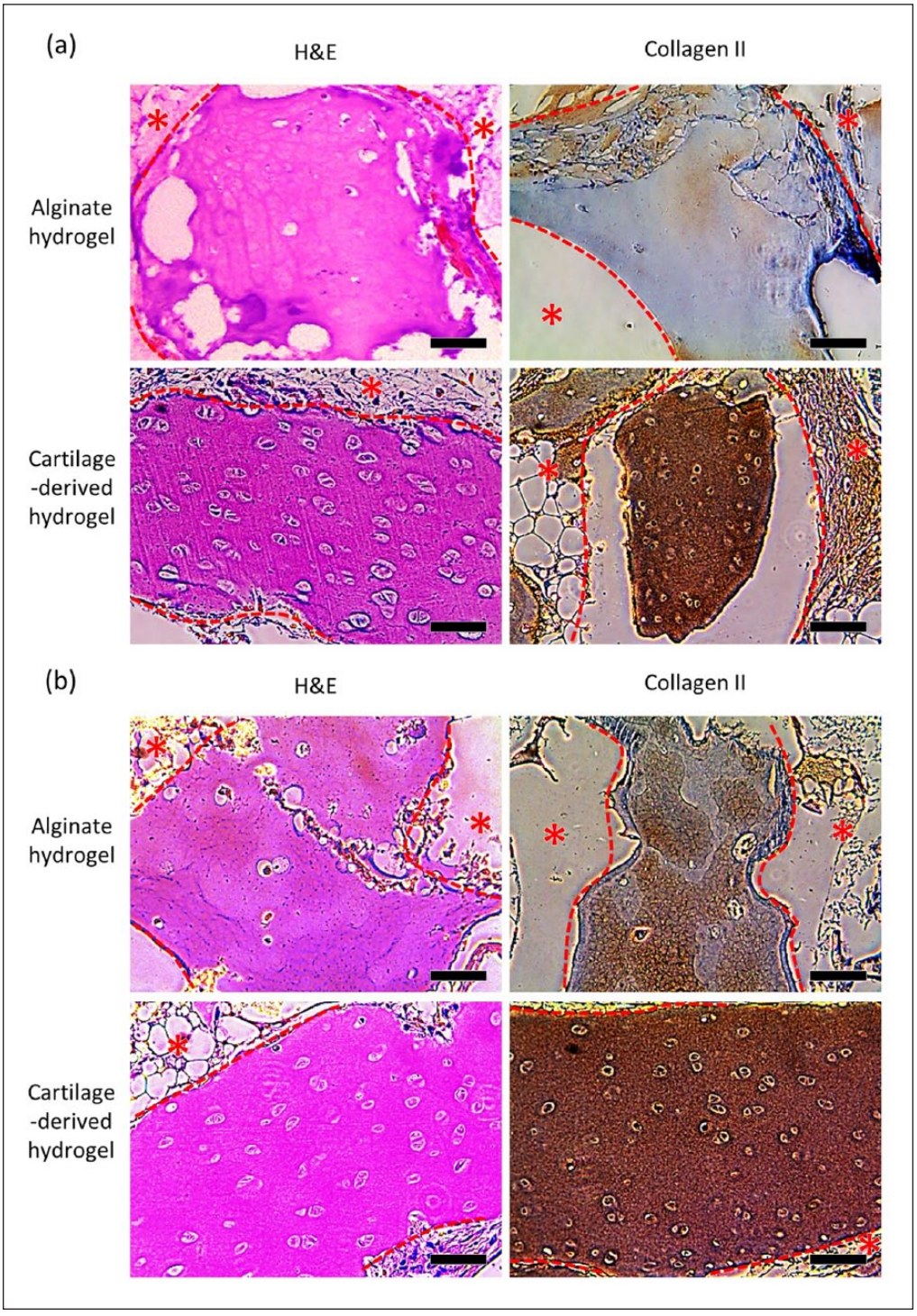

Figure 6. The histological analysis of the implanted engineered nasal cartilages. Representative images obtained after H&E and collagen II staining of the implants retrieved at (a) 6 and (b) 12 weeks (scale bars = 200 μm). The red dotted line and the star symbols indicate the PCL region.

of PCL. However, since PCL has a long-term degradation rate (>2 years), the neo-cartilage or neo-tissue would be expected to fill the cavities due to the degradation of PCL and eventually retain the nose shape.[25,26]

In the medical field, 3D printing has emerged as a powerful tool for the production of volumetric constructs according to patient-specific anatomy.[27–29] In particular, 3D printing–assisted prosthetic implants have been applied

to the reconstructions of cranial-maxillary-facial bone[30] and orbital wall defects.[31] The accurate 3D contours based on the patients' computed tomography (CT) data facilitated the reduction of surgery time and the geometrical errors between the implants and defects, and thereby reduced related complications. However, the prosthetic implants have less capability to repair and regenerate tissues because these processes rely almost exclusively on the migration of the host tissues. Engineered tissue incorporated with cells and biomaterials has been spotlighted as an ideal graft due to the high regenerative efficiency resulting from the delivered cells.[23,32,33] However, to date, there are few studies on the development of engineered tissue with patient-specific design because of the difficulties in generating human-scale living tissue constructs.[34] As to the current limitations, the process presented here for generating patient-specific nasal cartilage is substantially different from the conventional approaches. The results provide a proof-of-concept for applying 3D printing technology to the development of custom-built engineered tissue.

To avoid the issues of a limited cell source and donor site morbidity, a combination of hASCs and decellularized porcine cartilage ECM was used. hASCs are readily available through lipoaspirates and have shown good therapeutic efficacy;[35] they have been reported to exhibit self-renewing and multipotential differentiation capacity, including chondrogenic, osteogenic, and adipogenic lineages.[36,37] Nevertheless, it is difficult to expect most of the delivered hASCs to differentiate into chondrocytes and accelerate the cartilage repair.[37] The autologous chondrocyte implant (ACI), which uses the patient's own healthy chondrocytes, has been successfully applied to articular cartilage regeneration.[38] In the procedure of ACI, the chondrocytes are enzymatically isolated from the patient's articular cartilage and are expanded *in vitro*.[38] The cells are reinjected into the defective area of cartilage. The chondrocytes obtained from ACI can also be good cell candidates to promote excellent hyaline cartilage regeneration.

Through the injection technique, the hASC-laden cartilage-derived ECM hydrogel filled all the interior architecture of the 3D-printed nasal implant. The high cell retention is essential for cells to perform their therapeutic effect.[39] As the conventional cell seeding method depends on manual technique, inconsistently distributed cells and low cell efficiency can occur, which impede tissue regeneration.[15,40] The hydrogel injection technique enables a large number of cells to be settled and evenly distributed throughout the nasal implant. Moreover, this technique is relatively simple, requires basic skills, and can be easily accessible in clinical scenarios.

To promote regenerative effect, high cell viability should be maintained for long-term culture prior to implantation. However, since the diffusion capacity is limited within 100–200 μm, large-sized constructs commonly suffer from central hypoxia, which has been regarded as one of the major concerns in the field of tissue engineering.[41] In this study, hypoxia was rarely generated in either the innermost or outermost portions of the nasal implant, implying that the interior octahedral architecture with relatively large space (2 mm × 2 mm × 2 mm unit size) enables the provision of sufficient oxygen and nutrients to the cells through the hydrogel, which allows the diffusion of the water-soluble molecules.

The cartilage-derived hydrogel showed superior capability for neo-cartilage formation of the encapsulated hASCs, even though the engineered tissue constructs were implanted into a subcutaneous region, which provides nearby adipose tissue, but not cartilage tissue. We speculated that the cartilage decellularized ECM was mainly responsible for the neo-cartilage formation, due to the highly conservative biochemical components (e.g., cell adhesion proteins, growth factors, GAGs, and other ECM molecules) favorable for cartilage tissue formation. Interestingly, the inner region of the implanted engineered nasal cartilage also showed avascular characteristics, as seen in native cartilage.

Conclusion

This work demonstrated the 3D printing of a customized nasal implant and cartilage tissue regeneration, using hASC-laden cartilage-derived hydrogel to improve current limitations of autologous nasal grafts and synthetic nasal implants for augmentative rhinoplasty. The customized design of a nasal implant with an octahedral architecture was generated by a CAD process that determines the geometrical difference between preoperative and postoperative nasal shapes. In particular, the employment of cartilage-derived hydrogel into a customized nasal implant brought a unique advantage that facilitates cartilage regeneration with patient-specific design. The 3D-printed implant mainly contributed the structural accuracy of the engineered nasal cartilage, and the cartilage-derived hydrogel provided a favorable biochemical environment for chondrogenic differentiation and neo-cartilage formation from hASCs. The established serial process for creating an engineered nasal cartilage implant could accomplish both structural and biological advantages. In the future, this approach is expected to have broad applications for engineering implants of other tissue types, due to the versatility of 3D-printing technology, availability of various tissue dECM materials, and the pluripotency of hASC.

Authors' Note

Yeong-Jin Cho is also affiliated to Powder & Ceramics Division, Korea Institute of Materials Science (KIMS), Changwon, Korea.

Acknowledgements

H.-G.Y., Y.-J.C., and J.W.J. contributed equally to this work.

Declaration of conflicting interests

The author(s) declared no potential conflicts of interest with respect to the research, authorship, and/or publication of this article.

Funding

The author(s) disclosed receipt of the following financial support for the research, authorship, and/or publication of this article: This work was supported by the National Research Foundation (NRF) of Korea grant funded by the Korea government (MSIP; grant no.: 2010-0018294). This research was supported by Basic Science Research Program through the National Research Foundation of Korea(NRF) funded by the Ministry of Education (No. 2015R1A6A3A04059015). This research was supported by the MSIP(Ministry of Science, ICT and Future Planning), Korea, under the "ICT Consilience Creative Program" (IITP-R0346-16-1007) supervised by the IITP(Institute for Information & communications Technology Promotion).

Supplemental material

Supplemental material for this article is available online.

ORCID iD

Dong-Woo Cho https://orcid.org/0000-0001-5869-4330

References

1. Vuyk H and Adamson P. Biomaterials in rhinoplasty. *Clin Otolaryngol Allied Sci* 1998; 23(3): 209–217.
2. Lin G and Lawson W. Complications using grafts and implants in rhinoplasty. *Oper Techn Otolaryngol: Head Neck Surg* 2007; 18(4): 315–323.
3. Tham C, Lai Y-L, Weng C-J, et al. Silicone augmentation rhinoplasty in an oriental population. *Ann Plas Surg* 2005; 54(1): 1–5.
4. Chuangsuwanich A and Lohsiriwat V. Augmentation rhinoplasty with custom-made s-shape silicone implant in Asians: a 15-year experience. *Indian J Plas Surg* 2013; 46(3): 533–537.
5. Gelaude F, Vander Sloten J and Lauwers B. Automated design and production of cranioplasty plates: outer surface methodology, accuracies and a direct comparison to manual techniques. *Comput Aided Design Appl* 2006; 3(1–4): 193–202.
6. Jung JW, Park JH, Hong JM, et al. Octahedron pore architecture to enhance flexibility of nasal implant-shaped scaffold for rhinoplasty. *Int J Precis Eng Man* 2014; 15(12): 2611–2616.
7. Kim DW, Shah AR and Toriumi DM. Concentric and eccentric carved costal cartilage: a comparison of warping. *Arch Facial Plast S* 2006; 8(1): 42–46.
8. Mendelson A, Ahn JM, Paluch K, et al. Engineered nasal cartilage by cell homing: a model for augmentative and reconstructive rhinoplasty. *Plast Reconstr Surg* 2014; 133(6): 1344–1353.
9. Jang J, Yi H-G and Cho D-W. 3D printed tissue models: present and future. *ACS Biomater Sci Eng* 2016; 2(10): 1722–1731.
10. Moscatiello F, Jover JH, Ballester MAG, et al. Preoperative digital three-dimensional planning for rhinoplasty. *Aesthet Plas Surg* 2010; 34(2): 232–238.
11. Das S, Pati F, Choi Y-J, et al. Bioprintable, cell-laden silk fibroin–gelatin hydrogel supporting multilineage differentiation of stem cells for fabrication of three-dimensional tissue constructs. *Acta Biomater* 2015; 11: 233–246.
12. Kim JH, Choi Y-J, Yi H-G, et al. A cell-laden hybrid fiber/hydrogel composite for ligament regeneration with improved cell delivery and infiltration. *Biomed Mater* 2017; 12(5): 055010.
13. Chang JW, Park SA, Park JK, et al. Tissue-engineered tracheal reconstruction using three-dimensionally printed artificial tracheal graft: preliminary report. *Artif Organs* 2014; 38(6): E95–E105.
14. Choi YJ, Kim TG, Jeong J, et al. 3D cell printing of functional skeletal muscle constructs using skeletal muscle-derived bioink. *Adv Healthc Mater* 2016; 5(20): 2636–2645.
15. Pati F, Jang J, Ha D-H, et al. Printing three-dimensional tissue analogues with decellularized extracellular matrix bioink. *Nat Commun* 2014; 5: 3935.
16. Panwar A and Tan LP. Current status of bioinks for micro-extrusion-based 3D bioprinting. *Molecules* 2016; 21(6): 685.
17. Jung JW, Kang H-W, Kang T-Y, et al. Projection image-generation algorithm for fabrication of a complex structure using projection-based microstereolithography. *Int J Precis Eng Man* 2012; 13(3): 445–449.
18. Kang H-W and Cho D-W. Development of an indirect stereolithography technology for scaffold fabrication with a wide range of biomaterial selectivity. *Tissue Eng Part C: Me* 2012; 18(9): 719–729.
19. Kang KS, Lee S-I, Hong JM, et al. Hybrid scaffold composed of hydrogel/3D-framework and its application as a dopamine delivery system. *J Control Release* 2014; 175: 10–16.
20. Yi HG, Kang KS, Hong JM, et al. Effects of electromagnetic field frequencies on chondrocytes in 3D cell-printed composite constructs. *J Biomed Mater Res A* 2016; 104(7): 1797–1804.
21. Thomson C and Mendelsohn M. Reducing the incidence of revision rhinoplasty. *J Otolaryngol* 2007; 36(2): 130–134.
22. Crosara PFTB, Nunes FB, Rodrigues DS, et al. Rhinoplasty complications and reoperations: systematic review. *Int Arch Otorhi* 2017; 21(1): 97–101.
23. Yanaga H, Yanaga K, Imai K, et al. Clinical application of cultured autologous human auricular chondrocytes with autologous serum for craniofacial or nasal augmentation and repair. *Plast Reconstr Surg* 2006; 117(6): 2019–2030.
24. Ahn J, Honrado C and Horn C. Combined silicone and cartilage implants: augmentation rhinoplasty in Asian patients. *Arch Facial Plast S* 2004; 6(2): 120–123.
25. Park SH, Yun BG, Won JY, et al. New application of three-dimensional printing biomaterial in nasal reconstruction. *Laryngoscope* 2017; 127(5): 1036–1043.
26. Sun H, Mei L, Song C, et al. The in vivo degradation, absorption and excretion of PCL-based implant. *Biomaterials* 2006; 27(9): 1735–1740.
27. Gerstle TL, Ibrahim AM, Kim PS, et al. A plastic surgery application in evolution: three-dimensional printing. *Plast Reconstr Surg* 2014; 133(2): 446–451.
28. Park SH, Choi Y-J, Moon SW, et al. Three-dimensional bioprinted scaffold sleeves with mesenchymal stem cells for enhancement of tendon-to-bone healing in anterior cruciate ligament reconstruction using soft-tissue tendon graft. *Arthroscopy* 2018; 34(1): 166–179.
29. Rankin TM, Giovinco NA, Cucher DJ, et al. Three-dimensional printing surgical instruments: are we there yet? *J Surg Res* 2014; 189(2): 193–197.
30. Jardini AL, Larosa MA, Maciel Filho R, et al. Cranial reconstruction: 3D biomodel and custom-built implant created using additive manufacturing. *J Cranio Maxill Surg* 2014; 42(8): 1877–1884.
31. Stoor P, Suomalainen A, Lindqvist C, et al. Rapid prototyped patient specific implants for reconstruction of

orbital wall defects. *J Cranio Maxill Surg* 2014; 42(8): 1644–1649.
32. Choi Y-J, Yi H-G, Kim S-W, et al. 3D cell printed tissue analogues: a new platform for theranostics. *Theranostics* 2017; 7(12): 3118–3137.
33. Watson D and Reuther MS. Tissue-engineered cartilage for facial plastic surgery. *Curr Opin Otolaryngo* 2014; 22(4): 300–306.
34. Kang H-W, Lee SJ, Ko IK, et al. A 3D bioprinting system to produce human-scale tissue constructs with structural integrity. *Nat Biotechnol* 2016; 34(3): 312–319.
35. Zuk PA, Zhu M, Ashjian P, et al. Human adipose tissue is a source of multipotent stem cells. *Mol Biol Cell* 2002; 13(12): 4279–4295.
36. Bunnell BA, Flaat M, Gagliardi C, et al. Adipose-derived stem cells: isolation, expansion and differentiation. *Methods* 2008; 45(2): 115–120.
37. Estes BT, Diekman BO, Gimble JM, et al. Isolation of adipose-derived stem cells and their induction to a chondrogenic phenotype. *Nat Protoc* 2010; 5(7): 1294–1311.
38. Bentley G, Biant L, Carrington R, et al. A prospective, randomised comparison of autologous chondrocyte implantation versus mosaicplasty for osteochondral defects in the knee. *Bone Joint J* 2003; 85(2): 223–230.
39. Jang J, Park H-J, Kim S-W, et al. 3D printed complex tissue construct using stem cell-laden decellularized extracellular matrix bioinks for cardiac repair. *Biomaterials* 2017; 112: 264–274.
40. Kim YS, Shin YS, Choi JW, et al. The application of three-dimensional printing in animal model of augmentation rhinoplasty. *Ann Biomed Eng* 2015; 43(9): 2153–2162.
41. Jain RK, Au P, Tam J, et al. Engineering vascularized tissue. *Nat Biotechnol* 2005; 23(7): 821–823.